Xu Chen[1], Xiaoyong Zhuge[2,*], Xidi Zhang[1,3], Yuan Wang[1], and Daokai Xue[1]

[1]Key Laboratory of Mesoscale Severe Weather of Ministry of Education, and School of Atmospheric Sciences, Nanjing University, Nanjing, China.

[2]Nanjing Joint Institute for Atmospheric Sciences, Nanjing, China.

[3]National Meteorological Center, Beijing, China.

Corresponding author: Xiaoyong Zhuge (xyzhuge@yeah.net)

Key Points:

- The number of heavy precipitation northeastern China cold vortex (HPCV) events showed an upward linear trend in years 2001–2019.
- Most HPCV events lasted 2–5 days and those that moved into the study region lasted for longer.
- Precipitation was mostly concentrated within 2000 km southeast of the center of HPCV events.

Abstract

The northeastern China cold vortex (NCCV) has an important influence on the regional rainstroms over East Asia. Using the National Centers for Environmental Prediction Final (FNL) reanalysis dataset and the Global Precipitation Measurement product, an improved objective algorithm for identifying heavy precipitation NCCV (HPCV) events from 2001 to 2019 was designed. The climatological features of 208 HPCV events were investigated. The number of HPCV events showed an upward linear trend, with the highest frequency of occurrence in summer. The most active region of HPCVs was in the Northeast China Plain of 40–55° N. Most HPCV events lasted 2–5 days and had radii ranging from 250 to 1000 km. About 79% of the HPCV events was initiated (dissipated) in the definition region (35–60° N, 115–145° E). The initial position was close to the western boundary of the definition region, and the final position was mainly in the first and the fourth quadrants. The HPCV events that moved into the study region had a longer duration than those initiating in the region. The monthly variation of the strongest precipitation in the HPCV events showed a bimodal pattern, with two peaks in June and October. The location of the strongest precipitation was mostly concentrated within 2000 km southeast of the HPCV systems and it had a strong positive correlation with the center of HPCV events.

Plain Language Summary

A typical northeastern China cold vortex (NCCV) causing regional rainstroms is referred as to a heavy precipitation NCCV (HPCV) event. HPCV events were previously identified subjectively via painstaking manual analyses of daily weather charts; however, it can now be identified much faster using an automated algorithm. A dataset of HPCV events from 2001 to 2019 was established and their seasonal statistical characteristics were investigated. The number of

HPCV events had an increasing trend, implying a higher frequency of occurrence. HPCV events mainly occur over the Northeast China Plain and have an important influence on both the local weather conditions and remote regions.The heavy rainfall caused by HPCV events was more frequent in summer and autumn, and was mostly concentrated on the southeast side of the HPCV systems.

1 Introduction

Cut-off lows are isolated, closed cyclonic eddies with a cold core or cold troughs in mid- to high-latitude westerly winds. They have detached from a deep trough as a result of warm air masses cutting off their connection with colder air to the north (Palmen, 1949; Hsieh, 1949; Gimeno et al., 2007). Cut-off lows mainly occur in the mid- and upper troposphere. Their intensity decreases downward and few of them maintain cyclonic circulations in lower levels. Sometimes anticyclones can even be observed at the surface (Nieto et al., 2007). Porcu et al. (2007) showed that about 38% of cut-off lows in the Mediterranean region (25–55° N, 30° W–40° E) have well-defined cyclonic structures at ground level. Similarly, only 25% of cut-off lows in southern South America are associated with cyclonic circulations in the lower troposphere (Campetella & Possia, 2007).

There are three preferred regions of cut-off lows occurrence in the Northern Hemisphere, and the northeastern China is one of them (Nieto et al., 2005). Surrounded by mountains, the unique topography of northeastern China is prone to the formation of blocking systems. Moreover, northeastern China is located on the northern side of the upper level jet stream. The dynamic and thermal effects of the frontal jet are also conducive to the occurrence of cut-off lows (Wang et al., 2007). The northeastern China cold vortexes (NCCVs) are cut-off lows that occur over northeastern China.The currently widely used definition of NCCV events is proposed by Zheng et al. (1992) and Sun et al. (1994). A NCCV event should meet the following three criteria: (1) a low-pressure system accompanied by a cold core or an evident cold trough with at least one closed geopotential height contour at the 500 hPa isobaric surface; (2) the low-pressure system as defined in the first criteria located within the region (35–60° N, 115–145° E); and (3) the defined low-pressure system must last for more than three days within the study region. The definition emphasizes the configuration of the geopotential and temperature fields, as well as the continuity of the system (Wang et al., 2017).

Precipitation caused by westerlies, including NCCVs, is one of the main patterns of rainfall in East Asia (Zhao & Sun, 2007). The persistent activities of NCCVs have contributed to the increase of regional rainstorms in northeastern China (Sun et al., 2000; Xie et al., 2012). When interacting with other synoptic-scale systems, NCCVs can influence both the local weather conditions and remote regions. In South China, there is a positive correlation between NCCVs and rainfall during the pre-flood period. The anomalously strong NCCV is usually associated with a weak East Asian summer monsoon and a more southward western Pacific subtropical high, which provide the circulation conditions for

precipitation (Miao et al., 2006). Similarly, He et al. (2007) found a significant positive correlation between NCCVs and the amount of rainfall during the *meiyu* period, where strong NCCVs correspond to more *meiyu* rainfall and vice versa. The genesis, maintenance and dissipation of NCCVs therefore play important roles in feedback from the atmospheric circulations (Wang et al., 2007).

The precipitation caused by NCCVs can be understood as follows. As the cold center lags behind the geopotential center in the mid- to upper troposphere (e.g., 500 hPa), the system is baroclinic, forming cold advection behind the vortex. Unstable stratification will be established if the air conditions in the lower layer are warm and wet, which is necessary for heavy precipitation (Zhang & Li, 2009). During the time period June–August 1998, record floods occurred over Songhuajiang–Nenjiang region (Sun et al., 2002; Zhao & Sun, 2007). The most active NCCVs steered strong cold advection from west of Lake Baikal and Mongolia, while the summer monsoon transported moisture-rich current to northeast China. Another typical event occurred from July to August 2010, when seven of ten consecutive precipitation events were caused by the eastward movement of NCCVs (Sun et al., 2011). The cold air masses strongly converged with the warm moist current and continuously triggered new convective clouds under the impact of the local terrain (Liu et al., 2017).

NCCVs can also induce abrupt convective weather systems that produce thunderstorms, hail, heavy rainfall and other disastrous weather events (Li et al., 2016). The cold air masses in the mid- to high level are strong enough when a NCCV occur, and the characteristics of the lower troposphere are crucial in triggering convection. As long as there is heating on the ground (such as radiant heating), convection can be triggered. Strong convective weather systems are usually accompanied by heavy rainfall when there are sufficient amounts of low-level water vapor.

Previous studies have determined the climatological statistical characteristics of NCCVs. An early study was reported by Sun et al. (1994), who presented the spatial and temporal distribution of NCCVs during the time period 1956–1990. Hu et al. (2010) reported the seasonal climatology of NCCVs from 1979 to 2005, including features such as the spatial distribution, temporal variation, duration, radius and associated rainfall patterns over northeast China. Zhang et al. (2008) studied NCCVs in the warm season (May–September) when they were major high-impact weather systems. Most of these early studies focused on NCCVs before 2005. Huang and Li (2021) showed the characteristics of NCCVs in summer for a longer time period from 1979 to 2018, but the precipitation features were ignored. In addition, precipitation datasets used in these studies mostly came from weather stations in the surface meteorological observing network, with limited temporal and spatial resolution. Guo et al. (2021) investigated the Central Asian vortices influencing Xinjiang using 6 h precipitation datasets with a horizontal resolution of 5°. However, fine-scale precipitation products retrieved from satellites have not previously been reported in studies of NCCVs.

In this study, a precipitation dataset called Integrated Multi-satellite Retrievals for Global Precipitation Measurement (IMERG) project was used.It has a spatial resolution of $0.1° \times 0.1°$ at 30 min intervals. For convenience, only typical NCCV events with heavy rainfall—namely, heavy precipitation NCCV (HPCV) events—were selected and the key characteristics of HPCV eventswere investigated.

The remainder of this article is organized as follows. Section 2 introduces the data and methods for objectively identifying NCCV and HPCV events. Section 3 considers the seasonal characteristics of HPCV events and the characteristics of NCCV events are also given as a reference. Section 4 gives four types of HPCV events based on their positions. Section 5 investigates the characteristics of HPCV events related to precipitation. Conclusions and discussion are given in Section 6.

2 Data and Methodology

With $1° \times 1°$ grids every 6 h, the National Centers for Environmental Prediction (NCEP) Final (FNL) Operational Global Reanalysis dataset (Kalnay et al., 1996) was used for the objective identification of NCCV events. HPCV events were selected from the NCCV ones based on the IMERG precipitation dataset.

Available from June 2000, the IMERG dataset has three types of products (Early, Late and Final). Compared with the other two products, the Final product uses both forward and backward morphing and includes monthly gauge analysis, which is recommended for research studies. There are two types of precipitation dataset in Final product : precipitationCal (with gauge-adjusted processes) and precipitationUnCal (without gauge-adjusted processes). Guo et al. (2016) and Huang et al. (2018) showed that the precipitationCal dataset has less bias in estimating changes in precipitation over mainland China, so the precipitationCal dataset was used to identify HPCV events.

2.1 Algorithm for Identifying NCCV Events

The NCCV events can be recognized both subjectively and objectively. With the development of computer science, the painstaking visual inspection of thousands of daily weather charts has been gradually substituted by much faster objective procedures. According to the definition above, the identification of NCCV events mainly focuses on the configuration of the geopotential and temperature fields, as well as the continuity of the system. Zhang et al. (2008) detected NCCV events based only on the geopotential field, ignoring the influence of the temperature field. In their algorithm, if two cold vortex centers were within three grid points at adjacent times and the radial difference was 500 km, then they belonged to the same system. Hu et al. (2010) designed a three-step method with a positive zonal temperature Laplacian constraint. At any two consecutive times, two low-pressure grids were regarded as the same system only if the speed of movement was $<10°$ long./6 h. Wang et al. (2012) imitated the method of Nieto et al. (2005), introducing a thermal front parameter (TFP, $TFP = -\nabla|\nabla T| \bullet (\nabla T/|\nabla T|)$). Their tracking algorithm was from

Bell et al. (1989).

In addition to the geopotential and temperature fields, Jiang et al. (2012), Wang et al. (2012) and Huang and Li (2020) took the wind field into account. However, there is a quasi-geostrophic relationship at the mid- to high latitudes and the low-pressure center is basically equivalent to the cyclonic center. It is therefore not necessary to consider the wind field. In addition, some short-lived NCCV events can bring heavy rainfall. To identify these short-lived processes as accurately as possible, we lowered the threshold of the duration to two days, whereas other criteria still follow the definition of Zheng et al. (1992) and Sun et al. (1994).

The new automated algorithm is designed as follows.

1. A grid point is considered as a candidate NCCV center if its 500-hPa geopotential height is lower than that of the neighboring eight grid points. Most of the NCCVs have a maximum radius 1500 km (Hu et al., 2010). To ensure the positioning accuracy of the NCCV centers near boundaries, the study region (35–60° N, 115–145° E) extends temporarily outward by 15°—that is, (20–75° N, 100–160° E).

2. If there are multiple candidate NCCV centers in a 10° × 10° grid box, then the grid point with lowest geopotential height is retained, others are ruled out. At the same time, detected points not in the study region (35–60° N, 115–145° E) are discarded.

3. For the area surrounding the candidate NCCV center with a 15° radius, the temperature centroid (the mean latitude and longitude weighted by 500-hPa temperature) is calculated. The candidate NCCV center can be regarded as an NCCV center if the distance between it and the temperature centroid is 5°.

4. Similar to the tracking algorithm of Huang and Li (2020), the NCCV centers at any two consecutive synoptic hours (6 h) belong to the same system if the meridional distance is 5° and the zonal distance is 5° to the west (10° to the east). If multiple centers fit the criteria, then we take the nearest pair. The NCCV events must last for at least 48 h.

5. The fake NCCV centers caused by the extratropical transition of typhoons are removed manually.

The new algorithm comprehensively considers the features of NCCVs in geopotential and temperature fields. By introducing the concept of temperature centroid, the procedures of the algorithm are simplified and the operability is improved. The algorithm is also optimized to avoid ignoring NCCVs near the boundary and to discard the fake NCCVs caused by typhoons.

2.2 Algorithm for Identifing HPCV Events

A criterion, proposed by Sun et al. (2002), to determine whether NCCV events cause heavy precipitation was that: among 95 stations covering northeast China

(Liaoning, Jilin and Heilongjiang) and eastern Inner Mongolia (east of 115° E), at least three stations have the records of daily rainfall 50 mm from 1200 UTC to next 1200 UTC. In this study, a NCCV is defined as high-precipitation when the 24 h accumulated precipitation is 50 mm in the area around the system.

Based on the method of composite analysis, the IMERG precipitation and 500-hPa geopotential height were investigated to determine the rainfall range directly affected by NCCVs. Only NCCV samples in year of 2019 were selected if there are at least three grid points with IMERG precipitation greater than 16 mm h^{-1} in the 40° × 40° grid box. The composite result is shown in Figure 1. The distribution of rainstorms is comma-shaped and mainly in the east and south of the composite cold vortex. For the red dashed box extended 10° to the east and south from the blue dashed rectangle (the external rectangle around the outermost closed contour), a large area of precipitation can be included. The region covered by the red dashed rectangle is referred to here as the cold vortex rain area. Note that NCCVs are sometimes lack of a closed 4-dam-interval geopotential height contour, especially when they dissipate or move out of the study region. At this time, no attention is paid to the cold vortex rain area.

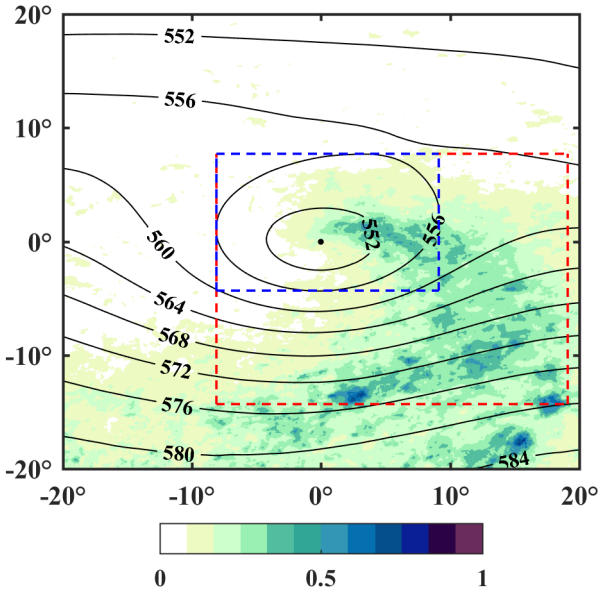

Figure 1. Composites of the IMERG precipitation (shading; units: mm h-1) and 500-hPa geopotential height (black contours; units: dam). The contour interval is 4 dam. The blue dashed box indicates the external rectangle around the outermost closed contour of the composite cold vortex. The red dashed rectangle defines the cold vortex rain area.

Because the earliest available IMERG data is from June 2000, the HPCV events are identified during the time period 2001–2019. Based on the analysis in Figure

1, the 24 h accumulated precipitation of NCCVs is calculated as the amount of IMERG rainfall in the ±12 h time period over cold vortex rain area, then a method consisting of the following two steps can be designed.

1. For the NCCV at a certain synopic hour every 6 h: The grid points with 24 h accumulated precipitation >0 mm are stored as list $\overrightarrow{\mathbf{N}}$. Then $\overrightarrow{\mathbf{N}}$ is sorted in descending order and the average value of the first 10% elements is calculated as P. The maximum value and size of $\overrightarrow{\mathbf{N}}$ are defined as M and S, respectively.

2. For the entire NCCV event: The number of synopic hours with M 50 mm and that of synopic hours of the entire NCCV process are counted. If their ratio is 70% and meanwhile at least one synopic hour satisfies both conditions that S is 1000 and P is 50 mm, then the NCCV event can be defined as a HPCV event.

Sun et al. (2002) mainly focused on the influence of NCCV events on northeast China. However, the active regions of NCCVs also include the Russian Far East, the Japanese islands and their adjacent sea areas. The definition of HPCV events by our algorithm is therefore more credible. As a result of the different resolution of precipitation datasets, the events identified by Sun et al. (2002) mostlycause local rainstorms, whereas HPCV events relate to regional rainstorms.

3 Seasonal Characteristics of HPCV Events

A total of 984 NCCV events and 208 HPCV events are identified using the two algorithms above, which means that about 21% of the NCCV events are defined as HPCV ones. This subsection presents temporal and spatial characteristics of the HPCV events, including their duration and size. For reference, the characteristics of general NCCV (GCV) events are also given. For clarify, a GCV (HPCV) day means the day with GCV (HPCV) occurrences hereafter. Spring refers to March–May (MAM), summer is June–August (JJA), autumn is September–November (SON) and winter is December–February (DJF).

3.1 Temporal Variations

The variation in the number of HPCV events is in good agreement with the number of HPCV days, with a correlation coefficient reaching 0.93 (Figure 2). Both the number of HPCV events and the number of HPCV days have a considerable interannual variability, with an upward linear trend during the time period 2000–2019. On average, HPCV events occur about 11 times per year over 43 days. A total of 18 HPCV events developed in both 2015 and 2017, whereas only four occurred in 2011. The number of HPCV days was highest in 2018 (66 days) and lowest in 2011 (19 days). The standard deviation of the number of HPCV and GCV events is 4.2 and 6.4 respectively, implying that the occurrence of HPCV events has a smaller interannual variability than GCV events. The GCV events were most active in 2012, with 64 events lasting for 199 days, and least active in 2003 and 2007.

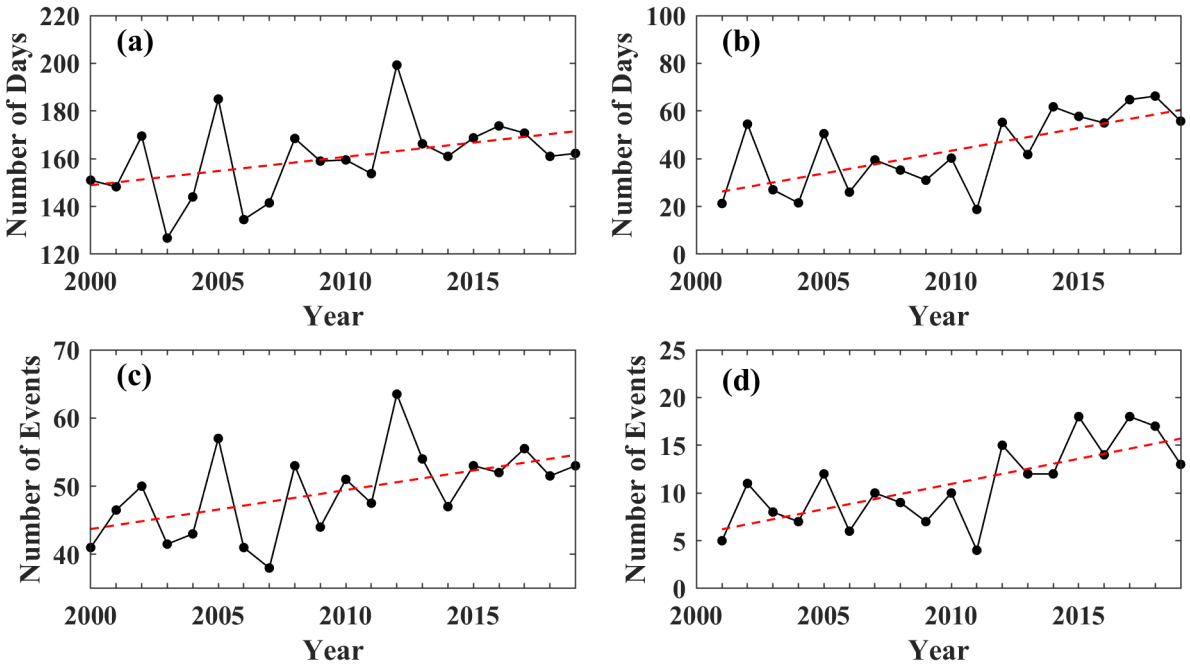

Figure 2. Year-to-year variation (black solid lines) and linear trend (red dashed lines) of the numbers of **(a, b)** days and **(c, d)** events during the time period 2000–2019. **(a, c)** GCV and **(b, d)** HPCV.

Figure 3 shows the monthly variation of cold vortex occurrences from 2000 to 2019. HPCV events occurred more often in summer and autumn. An average of five HPCV events occurred in summer, about 11–13 days per month, followed by autumn with three HPCV events. HPCV events were less common in the colder season, especially February–April. Figure 3b shows the ratio of HPCV occurrences to GCV occurrences in terms of days and events. From June to October, more than half of the GCV events were identified as HPCV ones. The reason for the high proportion is that the sufficient supply of moisture in summer and autumn favors the formation of unstable stratification, triggering convection and leading to precipitation. In contrast, the proportion is <10% in February–April. This is because the study region is dominated by cold dry air masses during late winter and early spring, and floods are unlikely to occur (Zhao & Sun, 2007).

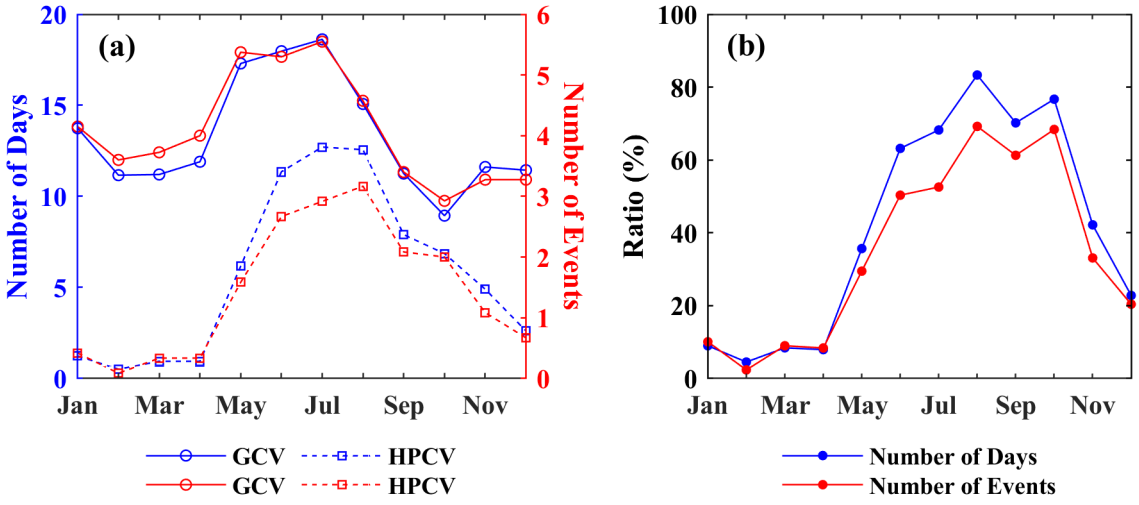

Figure 3. Monthly variations in **(a)** the number of GCV (HPCV) days (blue) and GCV (HPCV) events (red), and **(b)** ratio of HPCV occurrences to GCV occurrences in terms of days (blue) and events (red).

3.2 Spatial Distribution

As shown in Figure 4, GCVs and HPCVs are widespread over the study region and the main maximum core lies in the region 40–55° N, with a slightly southwest–northeast oriented band shape. Cold vortexes south of 40° N usually originate from subtropical jet streams with a shorter lifetime and smaller radius than those originating north of 40° N (Kentarchos & Davies, 1998). Likely to occur in regions of low terrain (Sun et al., 1994), GCVs are most concentrated over the Northeast China Plain, north of the Lesser Khingan Mountains and the Sea of Okhotsk. It is difficult for the moisture current to reach higher latitudes as a result of the blocking effect of the terrain. HPCVs are therefore only concentrated on the Northeast China Plain. The 20-year average position of HPCV is (48° N, 129.5° E), which is more southerly and westerly than that of the GCVs (49.86° N, 130.73° E).

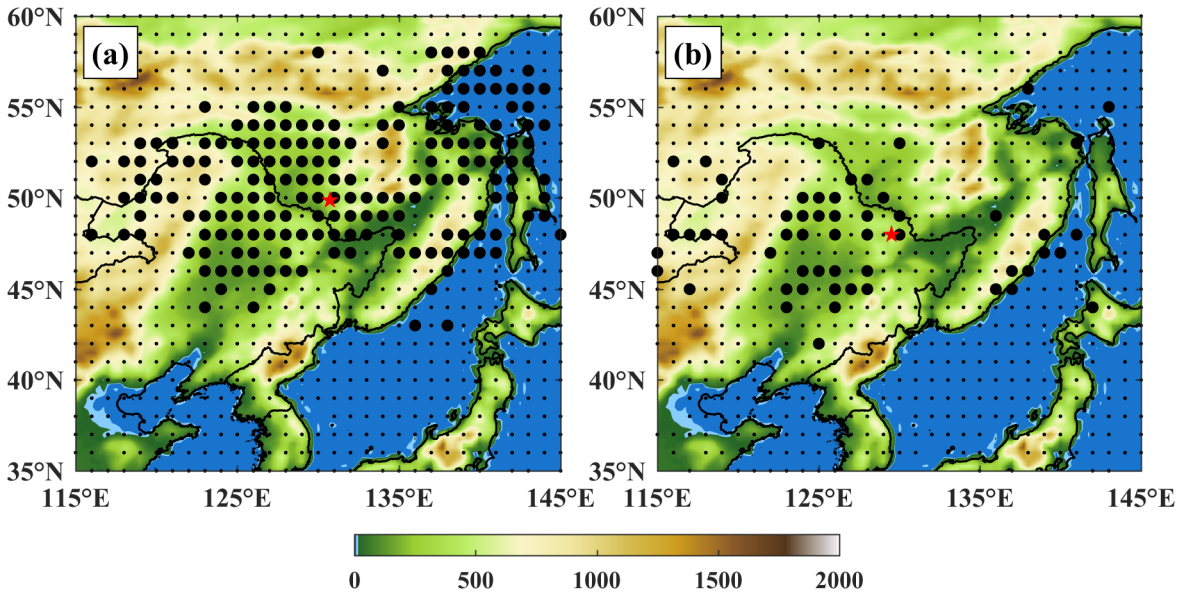

Figure 4. Spatial distribution of **(a)** GCV and **(b)** HPCV occurrences during 2000-2019. Large black dots indicate high frequencies (>25 and >10, respectively), whereas low frequencies are represented by small dots. The topography (shading; units: m) is from the ECMWF (the European Centre for Medium-Range Weather Forecasts) Reanalysis 5 dataset with a spatial resolution of 2.5° × 2.5°. The red star indicates the average position of cold vortex centers.

Figure 5a shows the variations in the zonal departure of GCVs and HPCVs from the average position. The central latitude of GCVs varies in the range of ±1.5°, and of ±0.5° after moving average. By contrast, the deviation of the HPCVs is obviously stronger than that of the GCVs. The latitudinal anomaly of most HPCV centers is ±2° and the maximum deviation can reach 4.13°. Both GCVs and HPCVs have shown a trend of northward movement since 2016.

The change in latitude of GCV occurrences in different seasons is investigated to explain the strong deviation of HPCVs (Figure 5b). The direction of deviation in summer and autumn is opposite to that in spring and winter, leading to a small annual variation of GCV occurrence latitudes. However, since 80.29% of the HPCV events occur in summer and autumn, the proportion of summer and autumn is greater than that of spring and autumn, which makes the annual latitudinal deviation of HPCV occurrence positions larger.

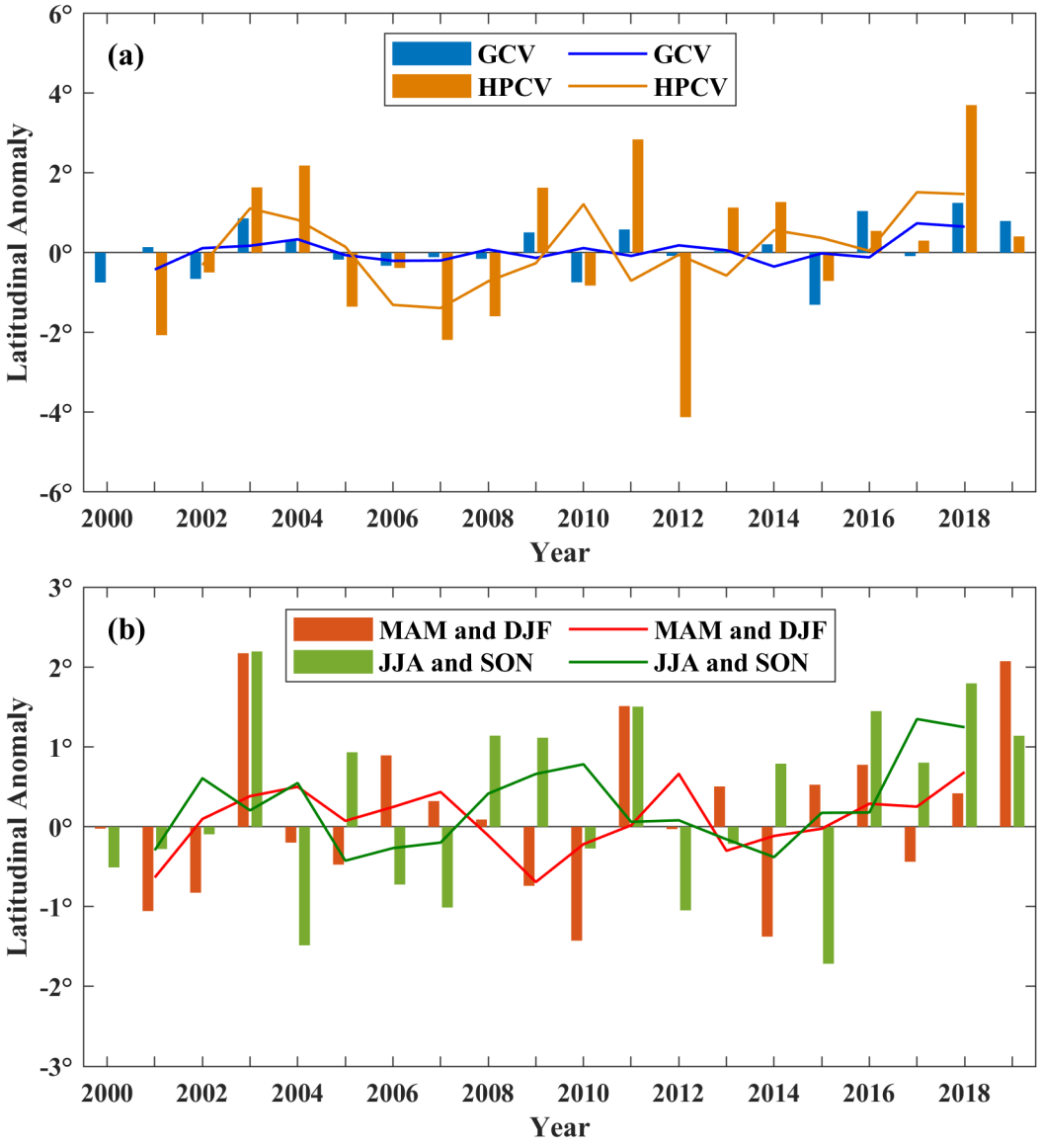

Figure 5. **(a)** Mean latitudinal anomaly of GCV and HPCV occurrences from 2000 to 2019 and its three-point moving average (solid lines). **(b)** Mean latitudinal anomaly of GCV occurrences in MAM and DJF (red) and JJA and SON (green) and its three-point moving average (solid lines).

3.3 Duration and Size

The duration of cold vortexes varies with the season (Figure 6). About 79.71%

of the HPCV events last 2–5 days and the longest process lasted 8.25 days. The HPCV events last a little longer than the GCV events, with the average duration of a HPCV event being 3.75 days and that of a GCV event 3.2 days. Seasonally, 14.81% of the HPCV events in MAM lasts 5 or more days, whereas the percentage lasting >5 days is 26.67% in JJA, 11.29% in SON and 23.08% in DJF. HPCV events in summer and winter are therefore likely to be longer than those in spring and autumn. Note that the duration of HPCV events is not equivalent to their lifetime. If the system moves in or out of the definition region, its lifetime is longer than detected. A more detailed classification is given in Section 4.

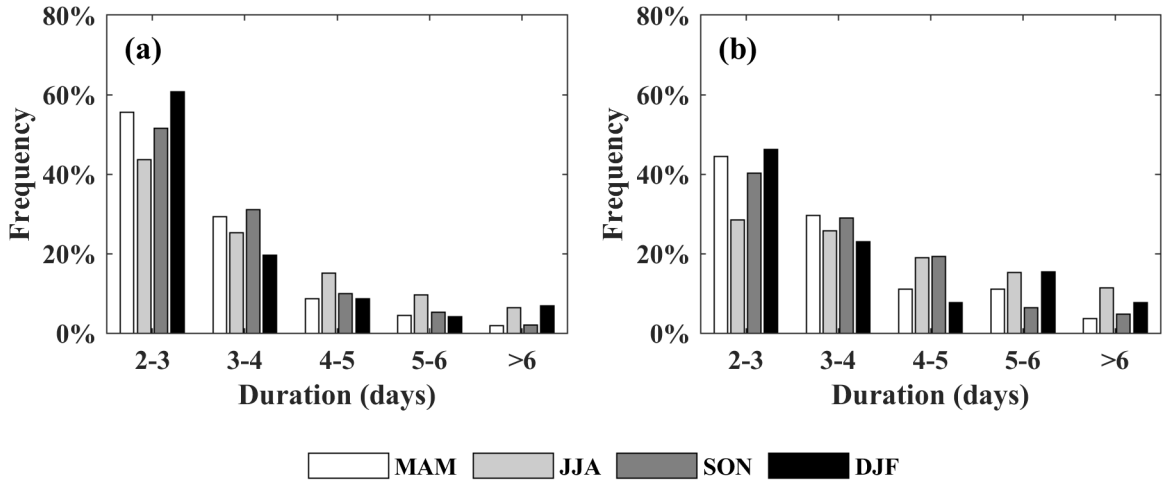

Figure 6. Frequency distribution of the duration of **(a)** GCV and **(b)** HPCV events in MAM, JJA, SON and DJF.

The size of a cold vortex is usually defined as the mean distance between the center and the outermost closed contour (Nielsen & Dole, 1992; Wen et al., 2021). Hu et al. (2010) marked the size of a cold vortex event by the longest dimension during its lifetime, which gives a larger radius. Here, we use the definition similar to Nielsen & Dole (1992) to describe the size of HPCVs (Figure 7). The radii of HPCVs are concentrated in the range 250–1000 km, which account for about 73.77% of the total number. By contrast, 72.62% of GCVs has a radius <750 km, implying that HPCVs are larger than GCVs. In winter, the percentage is largest when the radius of HPCVs is >1000 km. In summer and autumn, HPCVs tend to have a smaller radius between 250 and 500 km, which may be related to active convection suppressing the development of the cold vortexes.

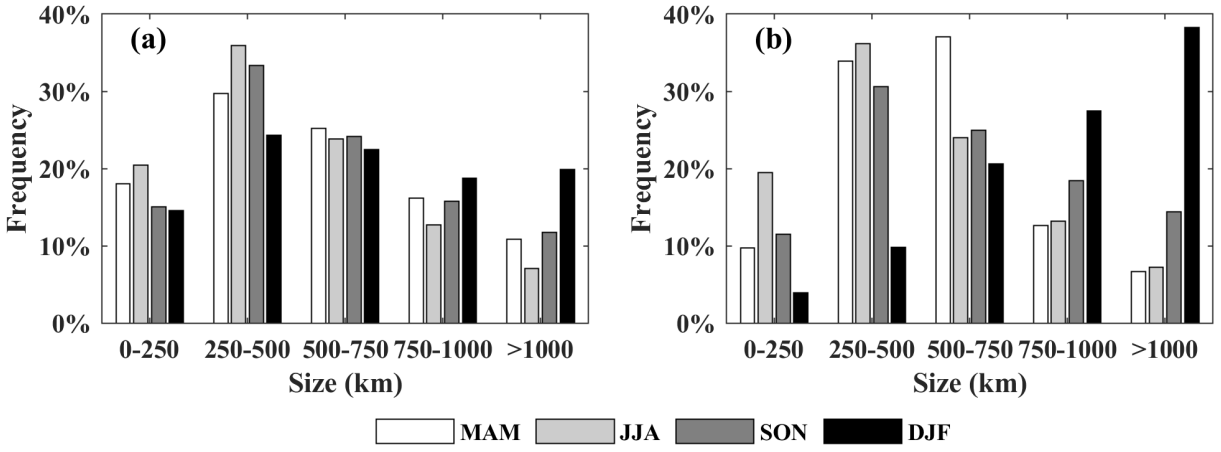

Figure 7. Frequency distribution of the size of **(a)** GCVs and **(b)** HPCVs in MAM, JJA, SON and DJF.

4 Classification of HPCV Events

HPCV events are divided into four categories: move-in, genesis, move-out and dissipation. The synoptic hour when a HPCV appears within the study region (35–60° N, 115–145° E) for the first (last) time is defined as the initial (final) time of a HPCV event. A cold vortex center is searched within a extended region (20–75° N, 100–160° E) at the last (next) synoptic hour of initial (final) time. If these two centers obtained at two consecutive synoptic hours (6 h) fit the tracking criteria proposed in Section 2.1, the HPCV event moves in (out) of the study region. Otherwise, the system belongs to the genesis (dissipation) type. Note that a HPCV event may belong to move-in/genesis types, and meanwhile move-out/dissipation types.

79.81% (78.85%) of HPCV events initiate (dissipate) within the definition region (Figure 8). The positions of some move-in (move-out) HPCV events are not on the boundary line as a result of the high temporal resolution. HPCV events mainly move in the region between 45 and 55° N near the western boundary. By contrast, the generated positions are widely distributed in all four quadrants and concentrated in the region 40–55° N near the western boundary. At the weakening stage, most HPCV events move out from the eastern boundary south of 55° N, whereas the positions of dissipation are mainly distributed in the first and fourth quadrants.

The tracks of HPCV events are disordered (figures omitted). Based on their initial and final positions, HPCV events move roughly eastward and southeastward. Qi et al. (1999) found that 81% of the cut-off lows in southern Australia moved either eastward or southeastward, whereas the remainder moved northward. Fang et al. (2021) considered the origins, movement directions and

movement velocities (distances) of GCV events, dividing their activity paths into four types: eastward movement; southeastward long-distance movement; eastward less-movement; and southward less-movement. The greatest number of GCV events were of the eastward movement type.

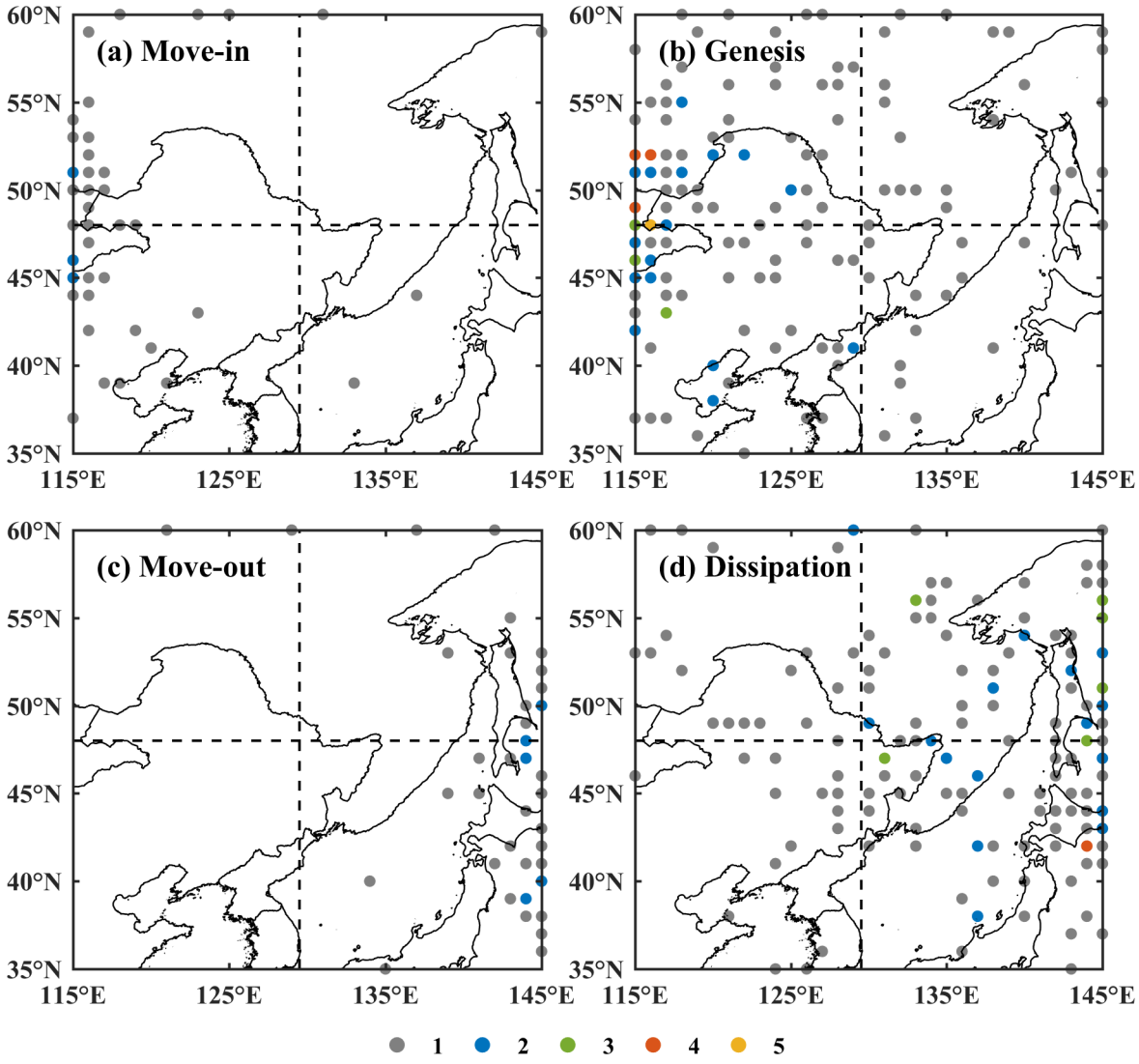

Figure 8. **(a, b)** Initial and **(c, d)** final positions of HPCV events. The gray, blue, green, red and yellow dots indicate 1–5 HPCV events, respectively. The dashed lines divide the region into four quadrants based on the average position of HPCV events.

Figure 9 shows the duration of four HPCV types. When the HPCV events last 2–3 days, the proportion of the genesis type (38.55%) is higher than that of move-in type (23.81%). The opposite results are obtained when the HPCV events last >4 days, as move-out and dissipation type accounts for 47.62 and 34.94% respectively. HPCV events moving in the study region therefore have a longer duration than that those initiating in the study region. However, there is no significant difference for HPCV events moving out of the region or dissipating within the region, suggesting that the weakening stage of HPCV events has little effect on their duration.

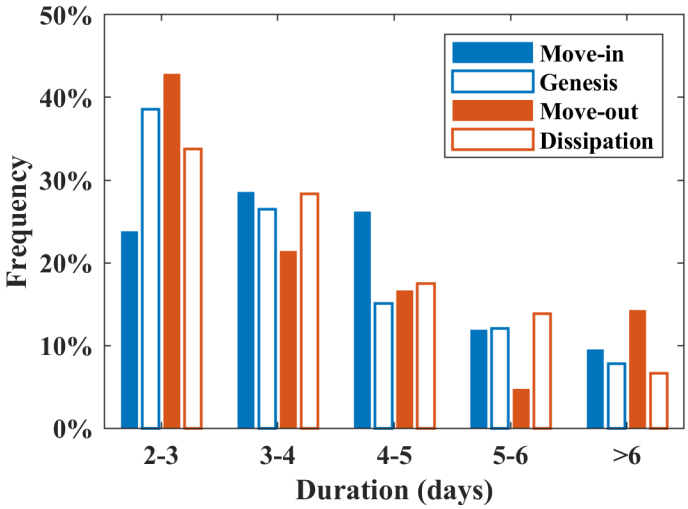

Figure 9. Frequency distribution of the duration of the move-in, genesis, move-out and dissipation types.

5 Precipitation Characteristics of HPCV Events

For a certain HPCV event, the maximum 24 h accumulated precipitation over the cold vortex rain area from the initial time to the final time is defined as the strongest precipitation. Figure 10 shows the yearly and monthly variations in the strongest precipitation. The strongest precipitation has a considerable interannual variability and a slight upward linear trend during the time period 2001–2019, with an average of 74.87 mm. The greatest precipitation was 98.96 mm in 2016. The two lowest precipitation years were 2003 (61.32 mm) and 2011 (61.36 mm). The monthly variation of the strongest precipitation shows a bimodal pattern. The two peaks occur in June and October, whereas the amount of strongest precipitation in July is relatively small. In winter, the strongest precipitation of HPCV events is low, especially in February, when it is only 59.79 mm.

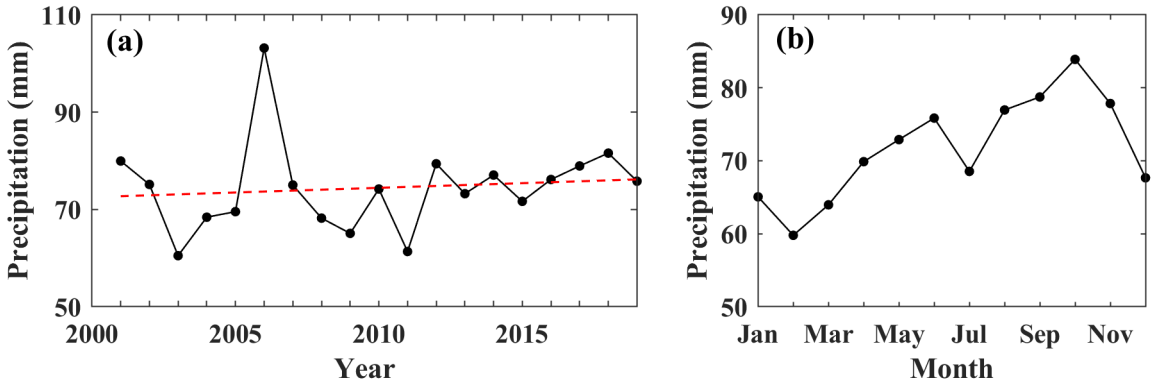

Figure 10. **(a)** Year-to-year variation (black solid line) and its linear trend (red dashed line) and **(b)** monthly variation of the strongest precipitation (units: mm) of HPCV events from 2001 to 2019.

The distribution of the strongest precipitation is shown in Figure 11a. The areas in which the strongest precipitation falls are mainly in the southeast of the study region, namely the Sea of Japan and its vicinity. With the abundant supply of moisture and the flat underlying surface, the ocean provids better conditions for regional rainstorms than the land surface, and there is relatively less precipitation on land. When the strongest precipitation in HPCV events is >100 mm, the location tends to be to the south, mainly south of 45°. The 19-year average position of the strongest precipitation is (40.95° N, 139° E), which is 11.83° further southeast than that of the center of HPCV events.

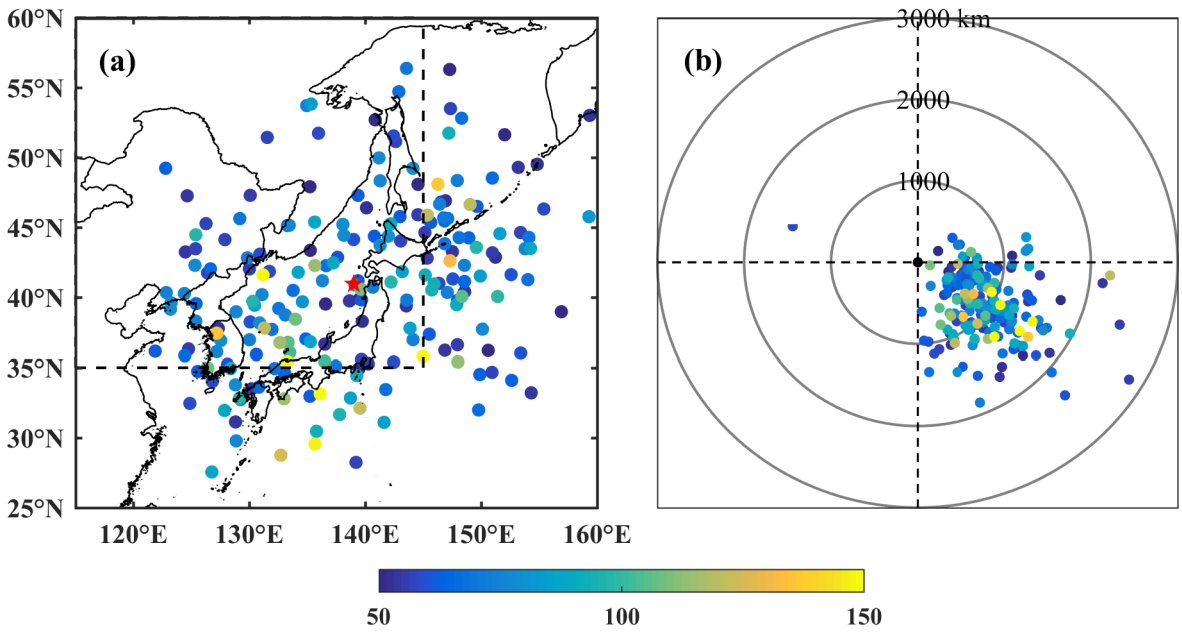

Figure 11. **(a)** Geographical locations of the strongest precipitation (units: mm). The dashed box indicates the study region. The red star indicates the average position of these locations. **(b)** The distribution of the strongest precipitation (units: mm) with the center of HPCV events as the origin. The gray circles indicate the distance from the center to 1000, 2000 and 3000 km.

There is a strong positive correlation between the location of the strongest precipitation and the center of HPCV events. The correlation coefficients are 0.84 in latitude and 0.78 in longitude (Figure 12). However, this does not mean that the strongest precipitation is evenly distributed around the center of HPCV events. It is mostly concentrated within 2000 km southeast of the HPCV centers (Figure 11b). The distance between the location of strongest precipitation and the center of HPCV events varies greatly, with the average distance 1000.97 km. The maximum and minimum distances are 2828.77 and 143.86 km, respectively. When the amount of the strongest precipitation is >100 mm, its location is mostly about 1000 km from the center.

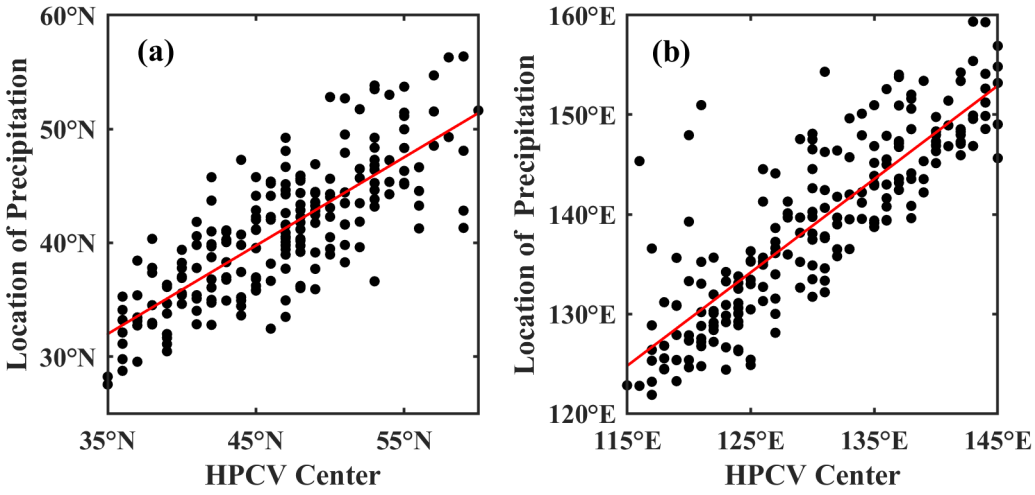

Figure 12. Scatter plot of the location of the strongest precipitation and the center of HPCV events in **(a)** latitude and **(b)** longitude. The red solid line is the linear fitting.

6 Conclusions and Discussion

In this study, by using the NCEP FNL Reanalysis dataset and the IMERG precipitation product, 208 HPCV events were identified during the time period 2001–2019. The basic characteristics of HPCV events are showed. There are the main conclusions summarized as follows.

- Both the number of HPCV days and HPCV events show an upward linear trend from 2001 to 2019. There are more HPCV events in summer than in the other three seasons, with an average of 11–13 days per month.
- HPCVs are frequently concentrated on the Northeast China Plain at 40–55° N, which is related to the effect of terrain on the supply of moisture. The latitudinal deviation of HPCVs is large because 80.29% of events occur in summer and autumn.
- Most HPCV events last 2–5 days. The HPCV events in summer and winter are likely to last longer. A total of 73.77% of HPCVs have a radius of 250–1000 km. HPCVs tend to have a larger radius during the cold seasons.
- Most HPCV events are initiated (dissipated) within the definition region. The location of initiation mainly range between 40 and 55° N near the western boundary, whereas the events dissipate in the first and the fourth quadrants. HPCV events moving into the study region have a longer duration than those initiating in this region.
- The monthly variation of the strongest precipitation shows a bimodal pat-

tern, with two peaks in June and October. The regions in which the strongest precipitation falls are mainly on the sea surface. There is a strong positive correlation between the location of the strongest precipitation and the center of HPCV events, with precipitation mostlyconcentrated within 2000 km southeast of the cold vortex systems.

This article mainly focused on the statistical results for the climatological features of HPCV events. The differences between HPCV and GCV events in terms of structure and their mechanisms of formation and development are still unkown. The interactions between HPCV events and other systems (e.g., high- and low-level jets, low-level shear lines and cyclones) still need further study.

Cold Vortexes extend from the upper to lower troposphere, with relatively uniform air masses. They do not cause regional heavy rainfall without interaction with other systems. On the other hand, extratropical cyclones have a quasi-barotropic character at the occlusion stage, with low pressure at lower levels and an overlapping cut-off low at upper levels. Are the HPCV events identified in this study accompany with extratropical cyclones on the ground? The statistical relationship between HPCV events and extratropical cyclones would be the future research focus.

Acknowledgments

The authors thank the anonymous reviewers for their helpful comments and valuable suggestions, which improved the manuscript.This work was financially supported by the National Key R&D Program of China under grant 2018YFC1507302, the National Natural Science Foundation of China under grant 42175006, and the Basic Research Fund of CAMS under grant 2020R002.

Data Availability Statement

NCEP FNL Reanalysis dataset is available at https://rda.ucar.edu/datasets/ds083.2/index.html. The IMERG dataset is publicly available at https://disc.gsfc.nasa.gov/datasets/GPM_3IMERGHH_06/summary. The topography is extracted from the the ECMWF Reanalysis 5 dataset, which is available at https://cds.climate.copernicus.eu/cdsapp#!/dataset/reanalysis-era5-single-levels?tab=form. The lists of 20-year NCCVs and HPCVs are available for free at Zenodo via https://doi.org/10.5281/zenodo.5571340 (Chen and Zhuge, 2021).

References

Bell, G. D., & Bosart, L. F. (1989). A 15-Year Climatology of Northern Hemisphere 500 mb Closed Cyclone and Anticyclone Centers. *Monthly Weather Review*, *117(10)*, 2142-2164. https://doi.org/10.1175/1520-0493(1989)117%3c2142:AYCONH%3e2.0.CO;2

Campetella, C. M., & Possia, N. E. (2007). Upper-level cut-off lows in southern South America. *Meteorology and Atmospheric Physics*, *96(1-2)*, 181-191. https://doi.org/10.1007/s00703-006-0227-2

Fang, Y., Chen, H., Lin, Y., Zhao, C., & Zhou, F. (2021). Classification of Northeast China Cold Vortex Activity Paths in Early Summer Based on K-means Clustering and Their Climate Impact. *Advances in Atmospheric Sciences*, *38(3)*, 400-412. https://doi.org/10.1007/s00376-020-0118-3

Gimeno, L., Trigo, R. M., Ribera, P., & García, J. A. (2007). Editorial: Special issue on cut-off low systems (COL). *Meteorology and Atmospheric Physics*, *96(1)*, 1-2. https://doi.org/10.1007/s00703-006-0216-5

Guo, H., Chen, S., Bao, A., Behrangi, A., Hong, Y., Ndayisaba, F., et al. (2016). Early Assessment of Integrated Multi-Satellite Retrievals for Global Precipitation Measurement over China. *Atmospheric Research*, *176-177*, 121-133. https://doi.org/10.1016/j.atmosres.2016.02.020

Guo, N., Zhou, Y., & Yang, L. (2021). Statistical analysis of Central Asian vortices and their influence on precipitation in Xinjiang. *Atmospheric Research*, *249*, 105327. https://doi.org/10.1016/j.atmosres.2020.105327

He, J., Wu, Z., Jiang, Z., Miao, C., & Han, G. (2007). "Climate effect" of the northeast cold vortex and its influences on Meiyu. *Chinese Science Bulletin*, *52*, 671-679. https://doi.org/10.1007/s11434-007-0053-z

Hsieh, Y. P. (1949). AN INVESTIGATION OF A SELECTED COLD VORTEX OVER NORTH AMERICA. *Journal of Meteorology*, *6(6)*, 401-410. https://doi.org/10.1175/1520-0469(1949)006%3c0401:AIOASC%3e2.0.CO;2

Hu, K., Lu, R., & Wang, D. (2010). Seasonal climatology of cut-off lows and associated precipitation patterns over Northeast China. *Meteorology and Atmospheric Physics*, *106(1-2)*, 37-48. https://doi.org/10.1007/s00703-009-0049-0

Huang, W., Chang, Y., & Liu, P. (2018). Assessment of IMERG precipitation over Taiwan at multiple timescales - ScienceDirect. *Atmospheric Research*, *214*, 239-249. https://doi.org/10.1016/j.atmosres.2018.08.004

Huang, X., & Li, D. (2020). Objective identification method and variation characteristics of the Northeast China cold vortex from May to August of 1979-2018. *Acta Meteorologica Sinica*, *78(6)*, 945-961. https://doi.org/10.11676/qxxb2020.077. (in Chinese with English abstract)

Jiang, D., Wang, J., Yan, Q., Wang, P., & Lu, Y. (2012). Climatic characters of northeast cold vortex and its effect on air temperature in Liaoning province from May to September during 1961-2010. *Journal of Meteorology and Environment*, *28(2)*, 5-9. https://doi.org/10.3969/j.issn.1673-503X.2012.02.002. (in Chinese with English abstract)

Kalnay, E., Kanamitsu, M., Kistler, R., Collins, W., Deaven, D., Gandin, L., et al. (1996). The NCEP/NCAR 40-Year Reanalysis Project.*Bulletin of the American Meteorological Society*, *77(3)*, 437-472. https://doi.org/10.1175/1520-0477(1996)077%3c0437:TNYRP%3e2.0.CO;2

Kentarchos, A. S. , & Davies, T. D. (1998). A climatology of cut-off lows

at 200 hPa in the Northern Hemisphere, 1990-1994. *International Journal of Climatology*, *18(4)*, 379-390. https://doi.org/10.1002/(SICI)1097-0088(19980330)18:4%3c379::AID-JOC257%3e3.0.CO;2-F

Li, S., Ding, Z., Dai, P., Liu, Y., & Han, Y. (2016). Recent Advances in Research on Northeast China Cold Vortex. *Journal of Arid Meteorology*, *34(1)*, 13-19. https://doi.org/10.11755/j.issn.1006-7639(2016)-01-0013. (in Chinese with English abstract)

Liu, Y., Liang, Z., & Li, Y. (2017). Observational and Simulative Study of a Local Severe Precipitation Event Caused by a Cold Vortex over Northeast China. *Advances in Meteorology*, *2017*, 1-18. https://doi.org/10.1155/2017/2764340

Miao, C., Wu, Z., He, J., Chi, Y. (2006). The Anomalous Features of the Northeast Cold Vortex During the First Flood Period in the Last 50 Years and Its Correlation with Rainfall in South China. *Chinese Journal of Atmospheric Sciences*, *30(6)*, 1249-1256. https://doi.org/10.3878/j.issn.1006-9895.2006.06.19. (in Chinese with English abstract)

Nielsen, J. W., & Dole, R. M. (1992). A Survey of Extratropical Cyclone Characteristics during GALE. *Monthly Weather Review*, *120(7)*, 1156-1168. https://doi.org/10.1175/1520-0493(1992)120%3c1156:ASOECC%3e2.0.CO;2

Nieto, R., Gimeno, L., Añel, J. A., De la Torre, L., Gallego, D., Barriopedro, D., et al. (2007). Analysis of the precipitation and cloudiness associated with COLs occurrence in the Iberian Peninsula. *Meteorology and Atmospheric Physics*, *96(1)*, 103-119. https://doi.org/10.1007/s00703-006-0223-6

Nieto, R., Gimeno, L., De la Torre, L., Ribera, P., Gallego, D., García-Herrera, R., et al. (2005). Climatological Features of Cutoff Low Systems in the Northern Hemisphere. *Journal of Climate*, *18(16)*, 3085-3103. https://doi.org/10.1175/JCLI3386.1

Palmén, E. (1949). Origin and Structure of High Level Cyclones South of the Maximum Westerlies. *Tellus*, *1(1)*, 22-31. https://doi.org/10.1111/j.2153-3490.1949.tb01925.x

Porcù, F., Carrassi, A., Medaglia, C. M., Prodi, F., & Mugnai, A. (2007). A study on cut-off low vertical structure and precipitation in the Mediterranean region. *Meteorology and Atmospheric Physics volume*, *96*, 121–140. https://doi.org/10.1007/s00703-006-0224-5

Qi, L., Leslie, L. M., & Zhao, S. X. (1999). Cut-off low pressure systems over southern Australia: climatology and case study. *International Journal of Climatology*, *19(15)*, 1633-1649. https://doi.org/10.1002/(SICI)1097-0088(199912)19:15%3c1633::AID-JOC445%3e3.0.CO;2-0

Sun, J., Dai, K., & Fan, L. (2011). Analysis and Forecasting Technology on the Heavy Rainfall Processes in the Northeast China During July to August 2010. Meteorological Monthly, 37(7), 785-794. https://doi.org/10.7519/j.issn.1000-0526.2011.7.002. (in Chinese with English abstract)

Sun, L., An, G., Gao, Z., Tang, X., Ding, L., & Sheng, B. (2002). A COMPOSITE DIAGNOSTIC STUDY OF HEAVY RAIN CAUSED BY THE NORTHEAST COLD VORTEX OVER SONGHUAJIANG-NENJIANG RIVER BASIN IN SUMMER OF 1998. *Journal of Applied Meteorological Science*, *13(2)*, 156-162. https://doi.org/10.3969/j.issn.1001-7313.2002.02.003. (in Chinese with English abstract)

Sun, L., An, G., Lian, Y., Sheng, B., & Tang, X. (2000). A STUDY OF THE PERSISTENT ACTIVITY OF NORTHEAST COLD VORTEX IN SUMMER AND ITS GENRAL CIRCULATION ANOMALY CHARECTERISTICS. *Acta Meteorologica Sinica*, *58(6)*, 704-714. https://doi.org/10.3321/j.issn:0577-6619.2000.06.006. (in Chinese with English abstract)

Sun, L., & Wang, Q. (1995). A Composite Diagnostic Analysis of Cold Vortex of Storm-rainfall and Non-Storm Rainfall Types. *Meteorological Monthly*, *21(3)*, 7-10. https://doi.org/10.7519/j.issn.1000-0526.1995.3.002. (in Chinese with English abstract)

Sun, L., Zheng, X., & Wang, Q. (1994). THE CLIMATOLOGICAL CHARACTERISTICS OF NORTHEAST COLD VORTEX IN CHINA. *Journal of Applied Meteorological Science*, *5(3)*, 297-303. https://doi.org/CNKI:SUN:YYQX.0.1994-03-005. (in Chinese with English abstract)

Wang, C., Xu, H., Ren, L., & Chen, L. (2012). The objective identification method of northeast cold vortex. *Journal of Meteorology and Environment*, *28(2)*, 1-4. https://doi.org/10.3969/j.issn.1673-503X.2012.02.001. (in Chinese with English abstract)

Wang, D., Zhong S., Liu Y., Li, J., Hu, K., Yang, S., et al. (2007). Advances in the Study of Rainstorm in Northeast China. *Advances in Earth Science*, *22(6)*, 549-560. https://doi.org/10.3321/j.issn:1001-8166.2007.06.001. (in Chinese with English abstract)

Wang, W., Li, J., Hu, C., Li, J., & Jiao, M. (2017). A review of definition, identification and quantitative investigation on Northeast cold vortex. *Journal of the Meteorological Sciences*, *37(3)*, 394-402. https://doi.org/10.3969/2015jms.0092. (in Chinese with English abstract)

Wen, D., Li, Y., Zhang, D., Xue, L., & Wei, N. (2018). A Statistical Analysis of Tropical Upper-Tropospheric Trough Cells over the Western North Pacific during 2006-15. *Journal of Applied Meteorology and Climatology*, *57(11)*, 2469-2483. https://doi.org/10.1175/JAMC-D-18-0003.1

Xie, Z., & Bueh, C. (2015). Different Types of Cold Vortex Circulations over Northeast China and Their Weather Impacts. *Monthly Weather Review*, *143(3)*, 845-863. https://doi.org/10.1175/MWR-D-14-00192.1

Xie, Z., Bueh, C., Ji, L., & Sun, S. (2012). The Cold Vortex Circulation over Northeastern China and Regional Rainstorm Events. *Atmospheric and Oceanic*

Science Letters, *5(2)*, 134-139. https://doi.org/10.1080/16742834.2012.11446979

Zhang, C., Zhang, Q., Wang, Y., & Liang, X. (2008). Climatology of warm season cold vortices in East Asia: 1979-2005. *Meteorology and Atmospheric Physics*, *100(1-4)*, 291-301. https://doi.org/10.1007/s00703-008-0310-y

Zhang, L., & Li, Z. (2009). A Summary of Research on Cold Vortex over Northeast China. *Climatic and Environmental Research*, *14(2)*, 218-228. https://doi.org/10.3878/j.issn.1006-9585.2009.02.11. (in Chinese with English abstract)

Zhao, S., & Sun, J. (2007). Study on cut-off low-pressure systems with floods over Northeast Asia. *Meteorology and Atmospheric Physics*, *96(1)*, 159-180. https://doi.org/10.1007/s00703-006-0226-3

Zheng, X., Zhang, Y., & Bai, R. (1992). *Rainstorm in Northeast China*. Beijing: China Meteorological Press. (in Chinese)